Infrared photodissociation spectra and solvation structures of $Cu^+(H_2O)_n$ (n = 1–4)

Takuro Iino [a], Kazuhiko Ohashi [b,*], Yutaka Mune [a], Yoshiya Inokuchi [c,1], Ken Judai [c], Nobuyuki Nishi [c], Hiroshi Sekiya [b]

[a] *Department of Molecular Chemistry, Graduate School of Sciences, Kyushu University, Hakozaki, Fukuoka 812-8581, Japan*

[b] *Department of Chemistry, Faculty of Sciences, Kyushu University, Hakozaki, Fukuoka 812-8581, Japan*

[c] *Institute for Molecular Science, Myodaiji, Okazaki 444-8585, Japan*

Abstract

Coordination and solvation structures of the $Cu^+(H_2O)_n$ ions with n = 1–4 are studied by infrared photodissociation spectroscopy and density functional theory calculations. Hydrogen bonding between H_2O molecules is detected in $Cu^+(H_2O)_3$ and $Cu^+(H_2O)_4$ through a characteristic change in the position and intensity of OH-stretching transitions. The third and fourth waters prefer hydrogen-bonding sites in the second solvation shell rather than direct coordination to Cu^+. The infrared spectroscopy verifies that the gas-phase coordination number of Cu^+ in $Cu^+(H_2O)_n$ is two and the resulting linearly coordinated structure acts as the core of further solvation processes.

---

* Corresponding author. Fax: +81-92-642-2607.

E-mail address: kazu.scc@mbox.nc.kyushu-u.ac.jp (K. Ohashi).

[1] Present address: Department of Chemistry, Graduate School of Science, Hiroshima University, Higashihiroshima 739-8526, Japan

1. Introduction

The study of clustering processes around an ion in the gas phase enables us to elucidate the ion solvation at the atomic or molecular level. The determination of stepwise binding energies of a ligand to a metal ion (M^+) has provided insight into how the metal–ligand interaction changes with the number of ligands. The binding energies of H_2O to alkali metal ions in $M^+(H_2O)_n$ decrease monotonically and slowly with increasing n [1,2]; the trend is consistent with an electrostatic bonding mechanism. In contrast, successive hydration of certain transition metal ions exhibits anomalous behavior.

Holland and Castleman [3] obtained the stepwise binding energies of $H_2O\cdots Cu^+(H_2O)_{n-1}$ for n = 3–5 using high-pressure mass spectrometry. The energies for smaller n = 1–4 were measured in collision-induced dissociation (CID) experiments performed by Magnera et al. [4,5]. Several years later, Dalleska et al. [6] reexamined the same system using the CID technique, where the data were analyzed in a more refined way. To our surprise, the binding energy of the second H_2O is larger than that of the first and the additional waters are bound much more weakly than the first two.

Bauschlicher et al. [7–9] performed ab initio calculations on $Cu^+(H_2O)_n$ with n = 1–4 for determining the stepwise binding energies and explaining the anomalous behavior. They showed that the bonding of H_2O to Cu^+ is essentially electrostatic in origin. The electrostatic bonding is enhanced by hybridization of the 4s and 3d orbitals of Cu for reducing the metal–ligand repulsion, resulting in a two-fold linear coordination for the n = 2 ion. The third H_2O can either bind directly to Cu^+, or hydrogen-bond to a first-shell H_2O. Some of previous calculations [9] predicted that the former structure was lower in energy, while others [10–15] suggested the opposite. Information on the binding energy alone is not enough to discriminate the two structures definitively, because both structures are consistent with the sudden drop of the binding energy of the third H_2O.

In the present work, we apply infrared (IR) photodissociation spectroscopy [16,17] to $Cu^+(H_2O)_n$. The method has capability of probing the completion of the solvent shell, because the OH stretches of H_2O are extremely sensitive to the formation of hydrogen bonds

[15,16]. Density functional theory (DFT) calculations are also performed for predicting the IR spectra of $Cu^+(H_2O)_n$. The comparison of the experimental and theoretical results provides insight into the coordination and solvation structures of $Cu^+(H_2O)_n$.

2. Experimental and computational

The IR photodissociation spectra are measured by using a triple quadrupole mass spectrometer [18,19]. A mixture of water and argon is expanded through a pulsed nozzle. The second harmonic of a Nd:YAG laser is focused on to a rotating Cu rod placed 14 mm downstream of the nozzle; vaporized Cu^+ ions are picked up by neutral water clusters in the expansion. The first quadrupole mass filter isolates the parent ions of interest. After deflection through an ion bender, the ions are introduced into the second quadrupole ion guide and irradiated by an IR laser (Continuum, Mirage 3000). Since the IR laser beam is not focused, one-photon absorption is the dominant process. The resulting fragment ions are analyzed by the third quadrupole mass spectrometer. The spectra of $Cu^+(H_2O)_n$ are obtained by recording the yields of the $Cu^+(H_2O)_{n-1}$ fragment ions as a function of wavenumber of the IR laser. Rare-gas tagging technique is employed, when necessary, where the spectra of $Cu^+(H_2O)_n \cdot Ar$ are measured by monitoring the Ar loss channel. The technique reduces the internal energies of the ions and decreases bandwidths of the spectra.

Theoretical calculations are carried out with GAUSSIAN 03 program package [20] using the hybrid DFT method (B3LYP) with the 6-311+G(2df) basis set for Cu and 6-31+G(d) for other atoms. The geometries of $Cu^+(H_2O)_n$ are optimized without any symmetry constraints. The main purpose of the calculations is to predict theoretical IR spectra of $Cu^+(H_2O)_n$. The harmonic vibrational frequencies and IR absorption intensities are evaluated for comparing the results with the experimental spectra. The frequencies of all the vibrations of all the species are scaled with a factor of 0.9757, which is chosen to reproduce the average of the symmetric (3657 cm^{-1}) and antisymmetric (3756 cm^{-1}) OH-stretching frequencies of the gas-phase H_2O molecule.

3. Results and discussion

3.1. Review of structures of $Cu^+(H_2O)_1$ and $Cu^+(H_2O)_2$

Since the structures of $Cu^+(H_2O)_n$ have already been described in detail [7–15], we briefly review a number of points relevant to the present study. It is established that a planar C_{2v} structure (Fig. 1a) is the global minimum of $Cu^+(H_2O)_1$. The main interaction between Cu^+ and H_2O is the electrostatic attraction between the positive charge on Cu^+ and the permanent dipole moment of H_2O. When the oxygen atom of H_2O approaches the metal, exchange repulsion arises between the lone pairs of the oxygen atom and dσ electrons of Cu^+. The net bonding is a balance between the charge–dipole attraction and the exchange repulsion. The lowest-energy structure of $Cu^+(H_2O)_2$ has C_2 symmetry (Fig. 1b), where two H_2O molecules are located on opposite sides of Cu^+. The two-fold linear coordination is anomalously stable, where the binding energy of the second H_2O is larger than that of the first [4–6]. Bauschlicher et al. [7–9] attributed the anomaly to the ability of Cu to use 4s–3dσ hybridization for moving the electron density to a lobe perpendicular to the metal–ligand axis. This hybridization permits the first H_2O to feel a higher nuclear charge. The second H_2O can also see a higher nuclear charge if it approaches from the side opposite the first. The second bond can be stronger than the first one, because the first H_2O pays the energetic cost of hybridization. Indeed, the Cu–O bond length computed for $Cu^+(H_2O)_2$ is shorter than that for $Cu^+(H_2O)_1$. One may expect that the stronger metal–ligand interaction results in larger reduction of the OH stretching frequencies. Unfortunately, the present IR spectra are not well-resolved enough to make a comparison of the frequency reduction between $Cu^+(H_2O)_1$ and $Cu^+(H_2O)_2$.

3.2. $Cu^+(H_2O)_3$

Fig. 1c shows two structures of $Cu^+(H_2O)_3$ obtained from our DFT calculations. The third H_2O can either bind directly to Cu^+ in a (3+0) form (3I), or it can hydrogen-bond to one of the first-shell waters in a (2+1) form (3II). Here, n_1 and n_2 in (n_1+n_2) stand for the numbers of ligands in the first and second solvation shells, respectively. In the (3+0) form,

one of the Cu–O bonds is approximately 0.3 Å longer than the other two and the angle between the shorter bonds is 162°. The two-fold linear coordination seems to remain intact, which is stabilized through the 4s–3dσ hybridization. The third H_2O cannot be close to Cu^+ because of the exchange repulsion with the enhanced electron density in the lobe perpendicular to the O–Cu–O axis. It follows that the third H_2O binds much weakly than the first two. In the (2+1) form, on the other hand, the distance between the oxygen atoms of the hydrogen-bonded waters is 2.64 Å, which is approximately 0.2 Å shorter than that in the neutral water dimer. Since the charge on the Cu^+ ion polarizes the H-donating H_2O in the first shell, the hydrogen bond is substantially strong, which is called 'charge-enhanced' hydrogen bond [21]. The bond strength can be similar in magnitude to the typically stronger metal–ligand interaction, placing these interactions in direct competition. The competition between the two interactions has been investigated for several systems including $Cu^{2+}(H_2O)_n$ [21], hydrated alkali-metal ions [16], and hydrated alkaline-earth-metal ions [22–24].

For $Cu^+(H_2O)_3$, Bauschlicher et al. [9] reported that the (3+0) form was more stable than the (2+1) form based on RHF geometry optimizations. Subsequent theoretical studies [10–12] confined their attention to the (3+0) form. Feller et al. [13] found that the (2+1) form is by 13 $kJmol^{-1}$ more stable than the (3+0) form at the MP2/aug-cc-pVDZ level of theory and the energy difference increases to 15 $kJmol^{-1}$ with the larger aug-cc-pVTZ basis set. More recent calculations [14,15] also predicted that the (2+1) form is located at the global minimum. The results of these calculations are to be confirmed by experimental studies, but no data have been available other than the stepwise binding energies. Information on the binding energies alone is not enough to discriminate the two structures definitively.

Fig. 2 compares the IR photodissociation spectra of $Cu^+(H_2O)_3$ and $Cu^+(H_2O)_3 \cdot Ar$ with the theoretical spectra of 3I and 3II. The spectrum of 3I (Fig. 2c) exhibits the symmetric and antisymmetric OH stretches around 3620 and 3720 cm^{-1}, respectively. A new transition appears at 3084 cm^{-1} in the spectrum of 3II (Fig. 2d), which is due to the hydrogen-bonded OH stretch. The experimental spectrum of $Cu^+(H_2O)_3$ (Fig. 2a) shows

overlapping features in the region of the free OH stretches. In addition, two broad maxima are observed around 3035 and 3340 cm^{-1}. The appearance of these maxima is suggestive of hydrogen bonding between H_2O molecules. The position of the lower-frequency maximum is consistent with the 3084 cm^{-1} transition of 3II, but the integrated intensity relative to the free OH stretches in the 3500–3800 cm^{-1} region is not as strong as predicted for 3II (Fig. 2d). A convincing explanation for this is that 3I coexists and contributes to the intensity of the free OH stretches.

The energy of a photon in the 3000–3800 cm^{-1} region (35–45 $kJmol^{-1}$) is smaller than the $H_2O\cdots Cu^+(H_2O)_2$ bond dissociation energy (60–70 $kJmol^{-1}$) [3–6]. This means that we preferentially detect a hot subset of the ions with internal energies sufficient to break the $H_2O\cdots Cu^+(H_2O)_2$ bond following one-photon absorption. As a result, the spectral features are fairly broad, precluding a detailed analysis of the spectrum. Then we carry out the Ar-tagging experiment for reducing the internal energy of the ions. The spectrum of $Cu^+(H_2O)_3\cdot Ar$ (Fig. 2b) exhibits the most intense band at 2980 cm^{-1} and a weaker one around 3280 cm^{-1} besides the free OH stretches in the 3600–3750 cm^{-1} region. The 2980 and 3280 cm^{-1} bands correspond to the 3035 and 3340 cm^{-1} maxima in the spectrum of $Cu^+(H_2O)_3$, respectively. The 2980 cm^{-1} band can be undoubtedly assigned to the hydrogen-bonded OH stretch of 3II, but there is a slight difference in the frequency between the theory (3084 cm^{-1}) and the experiment (2980 cm^{-1}). This is because it is improper to use the scaling factor of 0.9757 for this transition. The best agreement with the experiment is achieved by using a smaller factor of 0.94 for scaling the hydrogen-bonded OH stretch. Finally, the 3280 cm^{-1} band remains to be assigned. One may expect a cyclic (2+1) form, where the third H_2O bridges the first-shell molecules by simultaneously bonding to both ones. The resulting bent hydrogen bonds might be less strong and the OH groups involved might give transitions in this region. Such a cyclic (2+1) form is actually possible for $Ag^+(H_2O)_3$ [25,26]. However, all attempts to identify a similar form of $Cu^+(H_2O)_3$ failed, as did the calculations by Feller et al. [13]. Then a remaining candidate for the 3280 cm^{-1} band is an overtone of the H_2O bending mode or a combination band involving the hydrogen-bonded OH stretch.

In the spectrum of $Cu^+(H_2O)_3 \cdot Ar$, the hydrogen-bonded OH stretch is much stronger than the free OH stretches; the overall features coincide well with those of 3II. The majority of the Ar-tagged $Cu^+(H_2O)_3$ ions take the hydrogen-bonded form 3II. Thus the Ar-tagging experiment verifies that the most stable structure of $Cu^+(H_2O)_3$ is the (2+1) form, as is predicted by the recent calculations [13–15].

3.3. $Cu^+(H_2O)_4$

Fig. 1d represents three (2+2) forms of $Cu^+(H_2O)_4$ obtained from DFT calculations. We confine our attention to the (2+2) forms, because the two-fold coordination is shown to be stable in the previous section. Actually, (3+1) and (4+0) forms were calculated to be less stable than 4I by 12 and 32 kJmol^{-1}, respectively, at the MP2/aug-cc-PVDZ level [13]. In 4I, the third and fourth waters are bound to different H_2O in the first shell, while they are bonded to the same H_2O in 4II. Two additional waters in 4III form the dimer, which bridges the first-shell waters through hydrogen bonds. Lee et al. [15] showed that 4II and 4III lie 8 and 25 kJmol^{-1} higher than the most stable 4I, respectively, from calculations at the MP2/6-31+G* level.

The IR photodissociation spectra of $Cu^+(H_2O)_4$ and $Cu^+(H_2O)_4 \cdot Ar$ are compared with the theoretical spectra of 4I–III in Fig. 3. In the spectrum of 4I (Fig. 3c), an intense transition is located at 3128 cm^{-1} with a weaker one at 3143 cm^{-1}, which are due to hydrogen-bonded OH stretches. The magnitude of the red shift upon hydrogen bonding is smaller than that of the corresponding transition of 3II (3084 cm^{-1}). The 3256 and 3280 cm^{-1} transitions of 4II (Fig. 3d) are due to the symmetric and antisymmetric stretches of the doubly H-donating H_2O, respectively. These transitions show smaller red shifts than the hydrogen-bonded OH stretches of 4I. Three types of H-donating OH groups are responsible for the transitions located at 3234, 3364, and 3570 cm^{-1} in the spectrum of 4III (Fig. 3e).

Two broad maxima are seen around 3060 and 3340 cm^{-1} in the hydrogen-bonded OH region of the experimental spectrum of $Cu^+(H_2O)_4$ (Fig. 3a). The integrated intensity of the former is much larger than that of the free OH stretches in the 3600–3750 cm^{-1} region, in

contrast to the case of $Cu^+(H_2O)_3$. Large part of the $Cu^+(H_2O)_4$ ions are hydrogen-bonded isomers under warm conditions without Ar tagging. The 3060 cm^{-1} maximum of $Cu^+(H_2O)_4$ collapses into a strong peak at 3000 cm^{-1} with a shoulder at 3045 cm^{-1} in the spectrum of $Cu^+(H_2O)_4 \cdot Ar$ (Fig. 4b). These features are assignable to the 3128 and 3143 cm^{-1} transitions of 4I, if we rescale the frequencies with a factor of 0.94 as discussed in the previous section. There are weak features in the 3150–3400 cm^{-1} region of the spectrum of $Cu^+(H_2O)_4 \cdot Ar$. These features may be due to 4II and 4III, which exhibit hydrogen-bonded OH stretches in this region. However, the predominant intensity of the 3000 cm^{-1} peak indicates that 4I is the most abundant species generated in the Ar-tagging experiment, and therefore, the most stable structure of $Cu^+(H_2O)_4$.

4. Conclusions

The previous measurements of the stepwise binding energies [3–6] and supporting theoretical calculations [7–9] showed that the two-fold linear coordination of $Cu^+(H_2O)_2$ is anomalously stable. The stability of the two-fold coordination is apt to force additional waters to form the second solvation shell through hydrogen bonding. Since the charge on Cu^+ polarizes the H-donating H_2O in the first shell, the resulting charge-enhanced hydrogen bond is substantially strong. Consequently, the third H_2O prefers the solvation through hydrogen bonding rather than the direct coordination to Cu^+, as is established by the IR spectroscopy of $Cu^+(H_2O)_3 \cdot Ar$ in this work. The IR spectra of $Cu^+(H_2O)_4$ and $Cu^+(H_2O)_4 \cdot Ar$ suggest that the $Cu^+(H_2O)_2$ subunit with the two-fold linear coordination acts as the core of further solvation. The analysis of the spectra for $Cu^+(H_2O)_n$ with $n \geq 5$ is under way for confirming this point.

Acknowledgements

This work was supported in part by "Nanotechnology Support Project" and Grant-in-Aid for Scientific Research (No. 17550014) of the Ministry of Education, Culture, Sports, Science, and Technology (MEXT), Japan.

References

[1] I. Džidic, P. Kebarle, J. Phys. Chem. 74 (1970) 1466.

[2] N. F. Dalleska, B. L. Tjelta, P. B. Armentrout, J. Phys. Chem. 98 (1994) 4191.

[3] P. M. Holland, A. W. Castleman Jr., J. Chem. Phys. 76 (1982) 4195.

[4] T. F. Magnera, D. E. David, J. Michl, J. Am. Chem. Soc. 111 (1989) 4100.

[5] T. F. Magnera, D. E. David, D. Stulik, R. G. Orth, H. T. Jonkman, J. Michl, J. Am. Chem. Soc. 111 (1989) 5036.

[6] N. F. Dalleska, K. Honma, L. S. Sunderlin, P. B. Armentrout, J. Am. Chem. Soc. 116 (1994) 3519.

[7] M. Rosi, C. W. Bauschlicher Jr., J. Chem. Phys. 90 (1989) 7264.

[8] M. Rosi, C. W. Bauschlicher Jr., J. Chem. Phys. 92 (1990) 1876.

[9] C. W. Bauschlicher Jr., S. R. Langhoff, H. Partridge, J. Chem. Phys. 94 (1991) 2068.

[10] L. A. Curtiss, R. Jurgens, J. Phys. Chem. 94 (1990) 5509.

[11] W. F. Schneider, K. C. Hass, R. Ramprasad, J. B. Adams, J. Phys. Chem. 100 (1996) 6032.

[12] A. M. El-Nahas, N. Tajima, K. Hirao, J. Mol. Struct. (Theochem) 469 (1999) 201.

[13] D. Feller, E. D. Glendening, W. A. de Jong, J. Chem. Phys. 110 (1999) 1475.

[14] J. V. Burda, M. Pavelka, M. Šimánek, J. Mol. Struct. (Theochem) 683 (2004) 183.

[15] H. M. Lee, S. K. Min, E. C. Lee, J.-H. Min, S. Odde, K. S. Kim, J. Chem. Phys. 122 (2005) 064314.

[16] J. M. Lisy, Int. Rev. Phys. Chem. 16 (1997) 267.

[17] M. A. Duncan, Int. Rev. Phys. Chem. 22 (2003) 407.

[18] Y. Inokuchi, N. Nishi, J. Chem. Phys. 114 (2001) 7059.

[19] Y. Inokuchi, K. Ohshimo, F. Misaizu, N. Nishi, Chem. Phys. Lett. 390 (2004) 140.

[20] M. J. Frisch et al., GAUSSIAN 03, Gaussian, Inc., Pittsburgh, 2003.

[21] A. J. Stace, Phys. Chem. Chem. Phys. 3 (2001) 1935.

[22] Y. Inokuchi, K. Ohshimo, F. Misaizu, N. Nishi, J. Phys. Chem. A 108 (2004) 5034.

[23] H. Machinaga, K. Ohashi, Y. Inokuchi, N. Nishi, H. Sekiya, Chem. Phys. Lett. 391 (2004) 85.

[24] K. Ohashi, K. Terabaru, Y. Inokuchi, Y. Mune, H. Machinaga, N. Nishi, H. Sekiya, Chem. Phys. Lett. 393 (2004) 264.

[25] E. C. Lee, H. M. Lee, P. Tarakeshwar, K. S. Kim, J. Chem. Phys. 119 (2003) 7725.

[26] T. Iino et al. (in preparation).

Figure Captions

Fig. 1. Stable structures of $Cu^+(H_2O)_n$ (n = 1–4) obtained from DFT calculations. Cu and O atoms are denoted by solid and shaded circles, respectively. Bond distances are in units of Å.

Fig. 2. Comparison of experimental IR spectra of (a) $Cu^+(H_2O)_3$ and (b) $Cu^+(H_2O)_3 \cdot Ar$ with theoretical IR spectra obtained from DFT calculations for (c) 3I and (d) 3II.

Fig. 3. Comparison of experimental IR spectra of (a) $Cu^+(H_2O)_4$ and (b) $Cu^+(H_2O)_4 \cdot Ar$ with theoretical IR spectra obtained from DFT calculations for (c) 4I, (d) 4II, and (e) 4III.

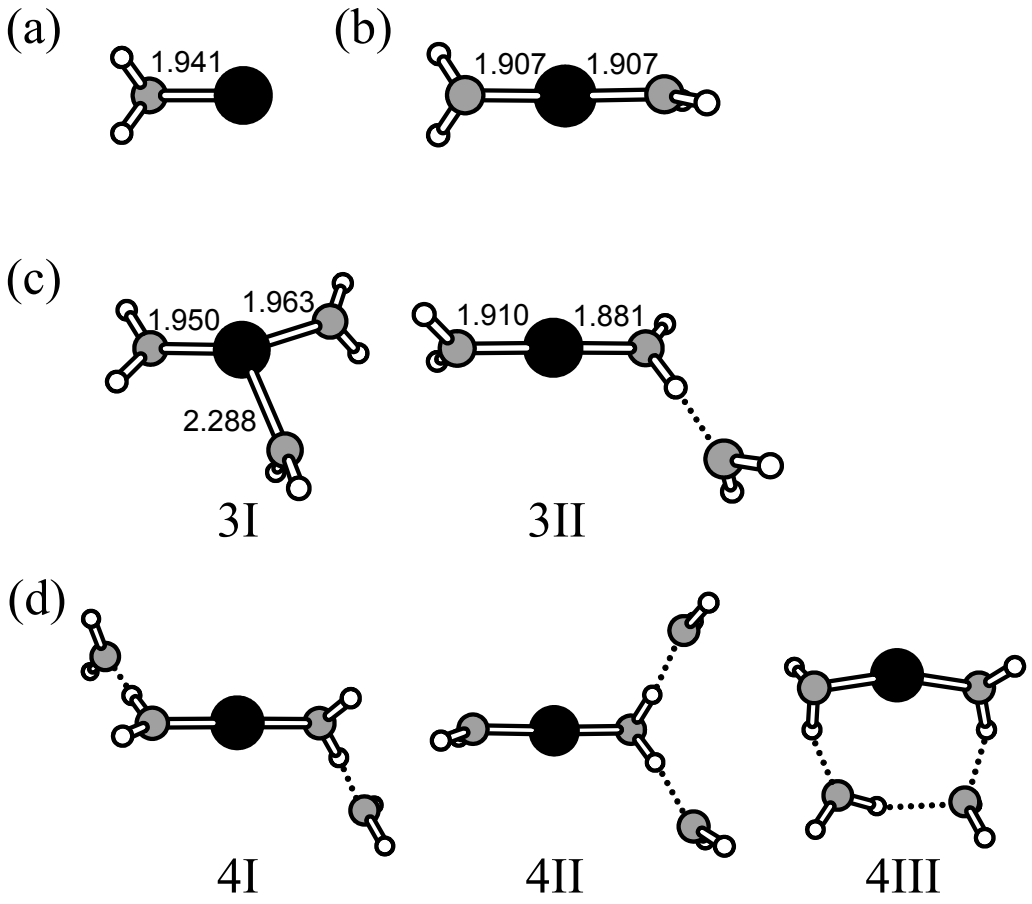

Fig. 1 Iino et al.

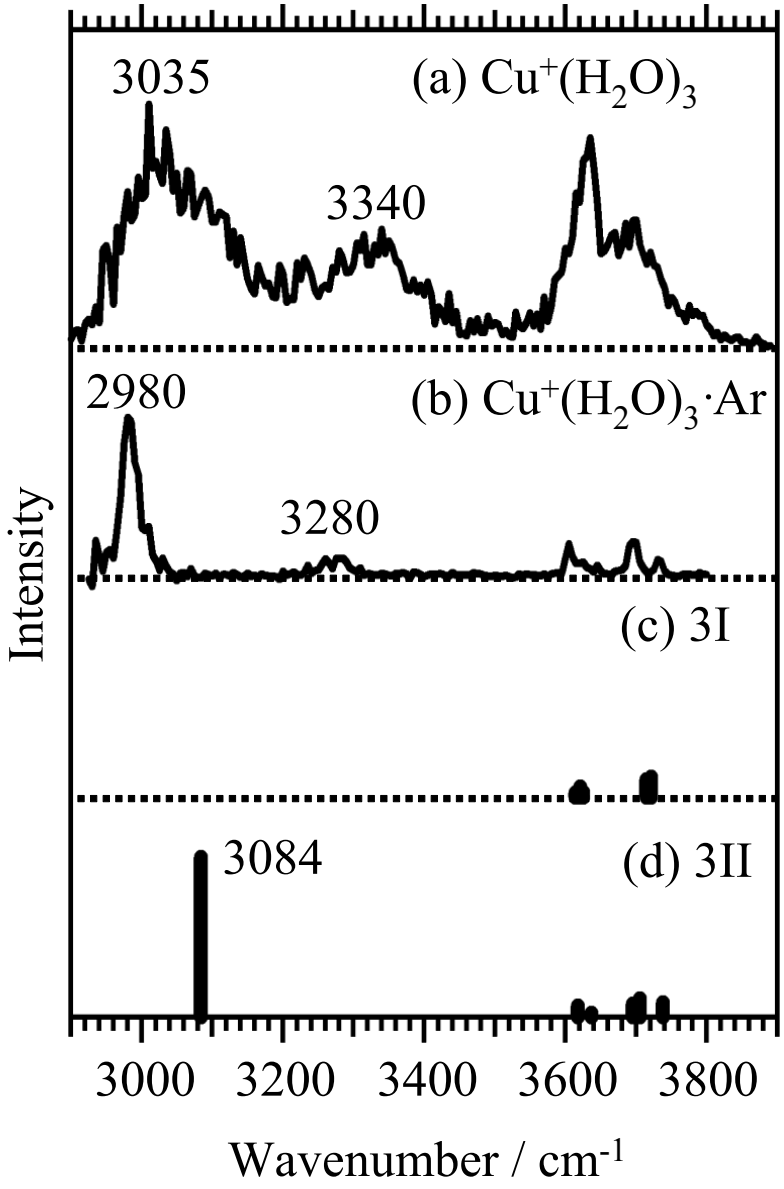

Fig. 2 Iino et al.

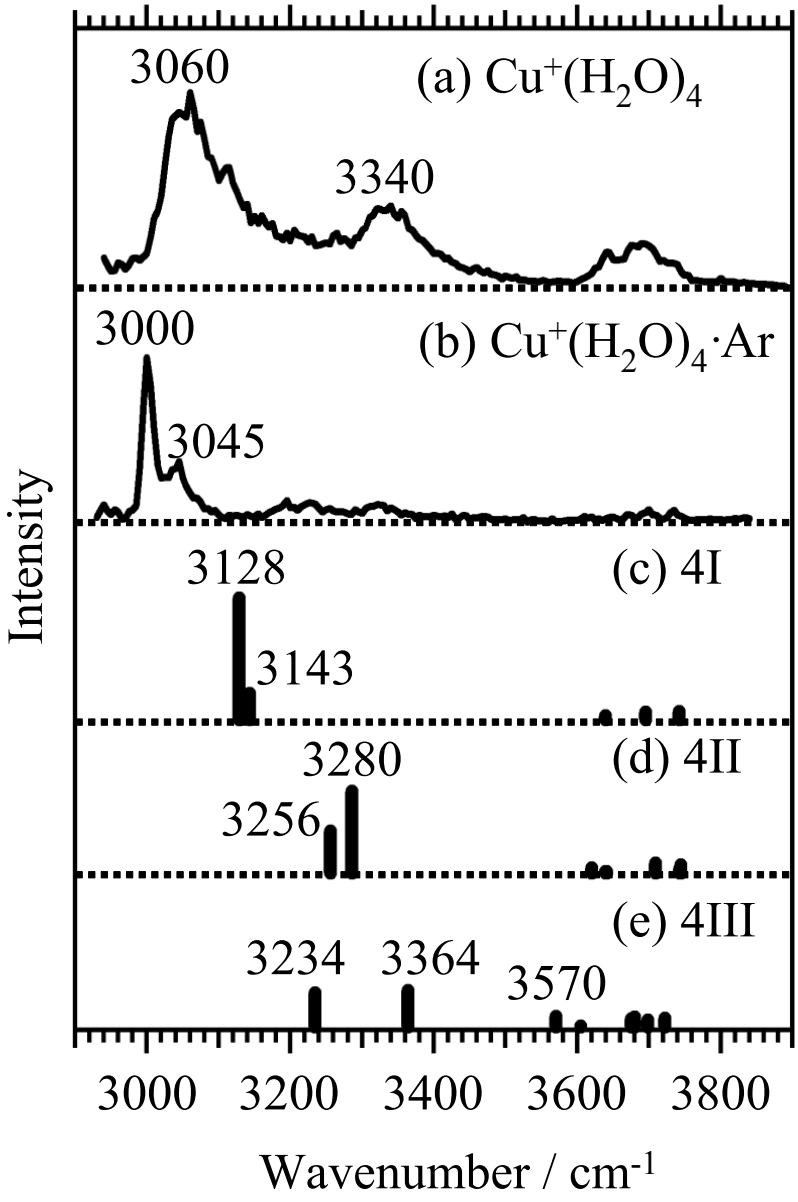

Fig. 3 Iino et al.

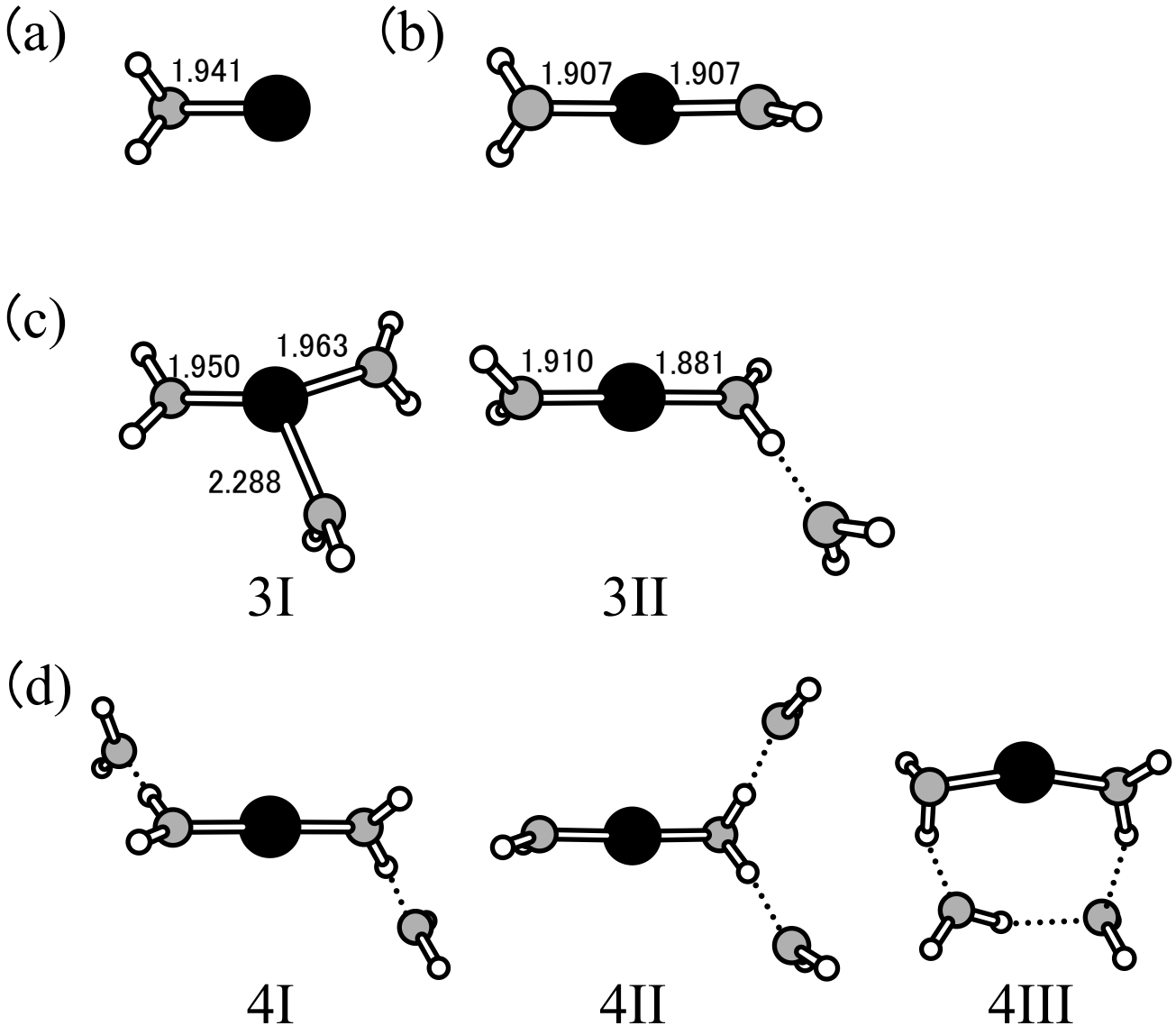

Fig. 1 Iino et al.

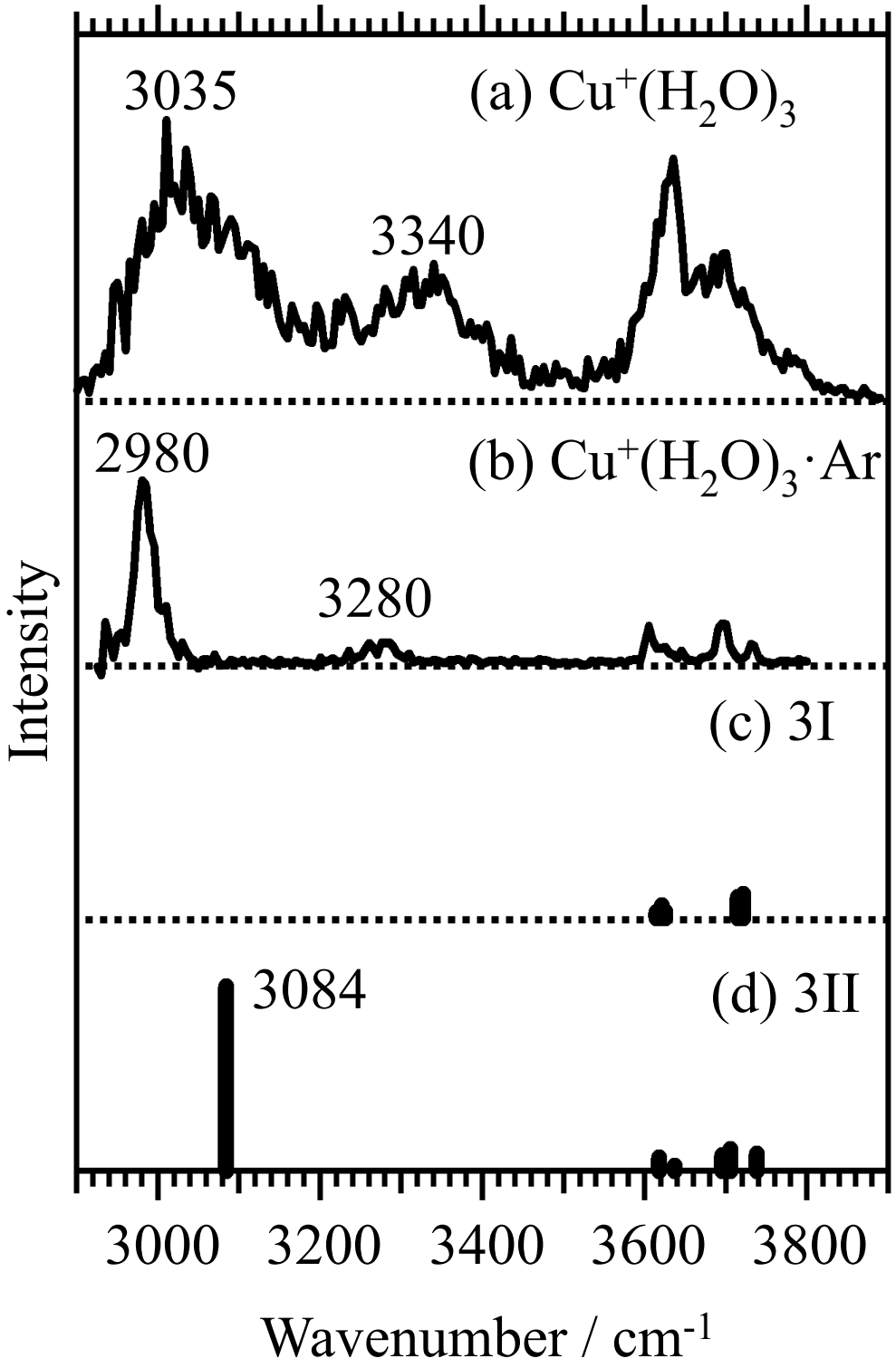

Fig. 2 Iino et al.

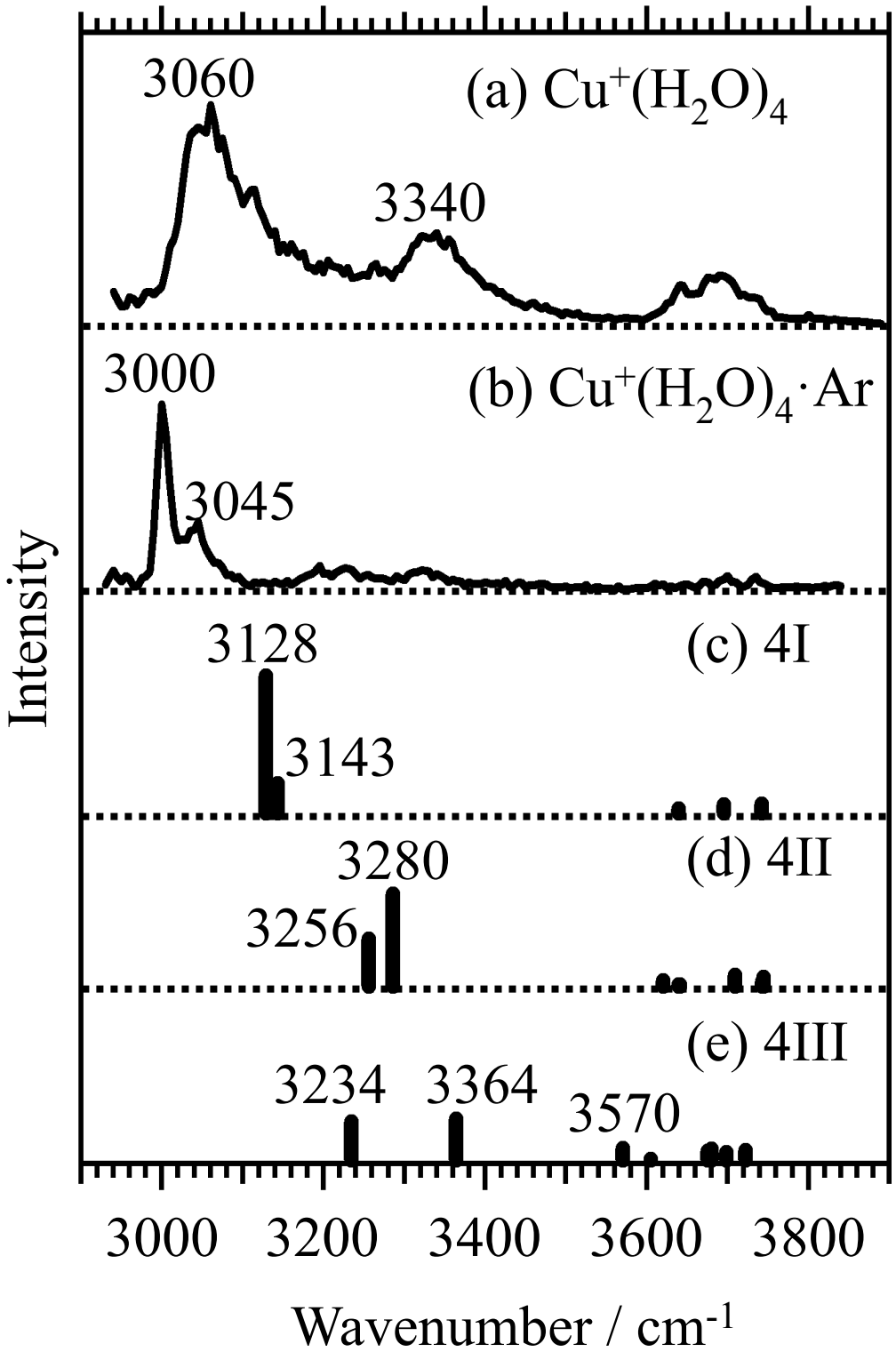

Fig. 3 Iino et al.